




The Role of Deposition Temperature in the Photovoltaic Properties of RF-Sputtered CdSe Thin Films

Hasrul Nisham Rosly^{1,2,*}, Kazi Sajedur Rahman^{3,*}, Siti Fazlili Abdullah¹, Muhammad Najib Harif¹, Camellia Doroody¹, Puvaneswaran Chelvanathan³, Halina Misran⁴, Kamaruzzaman Sopian³ and Nowshad Amin^{1,4,*}

- ¹ College of Engineering, Universiti Tenaga Nasional, Jalan IKRAM-UNITEN, Kajang, Selangor 43000, Malaysia; siti@uniten.edu.my (S.F.A.); najibharif@gmail.com (M.N.H.); cammydo@yahoo.com (C.D.)
- ² Faculty of Electrical and Electronic Engineering Technology, Universiti Teknikal Malaysia Melaka, Durian Tunggal, Melaka 76100, Malaysia
- ³ Solar Energy Research Institute, Universiti Kebangsaan Malaysia, Bangi, Selangor 43600, Malaysia; cpuvaneswaran@ukm.edu.my (P.C.); ksopian@ukm.edu.my (K.S.)
- ⁴ Institute of Sustainable Energy, Universiti Tenaga Nasional, Jalan IKRAM-UNITEN, Kajang, Selangor 43000, Malaysia; halina@uniten.edu.my
- * Correspondence: hasrul@utem.edu.my (H.N.R.); sajed@ukm.edu.my (K.S.R.); nowshad@uniten.edu.my (N.A.)

Abstract: Cadmium selenide (CdSe) thin films were grown on borosilicate glass substrates using the RF magnetron sputtering method. In this study, CdSe thin film was deposited at a deposition temperature in the range of 25 °C to 400 °C. The influence of deposition or growth temperature on the structural, morphological, and opto-electrical properties of CdSe films was investigated elaborately to achieve a good-quality window layer for solar-cell applications. The crystal structure, surface morphology, and opto-electrical characteristics of sputtered CdSe films were determined using X-ray diffraction (XRD), field emission scanning electron microscopy (FESEM), UV-Vis spectrophotometry, and Hall effect measurement, respectively. The XRD results revealed the polycrystalline nature of CdSe, with a hexagonal structure having a strong preferential orientation toward the (002) plane. As evident from the FESEM images, the average grain size and surface morphology of the films were dependent on deposition temperatures. The carrier concentration was obtained as 10^{14} cm^{-3} . The band gap in the range of 1.65–1.79 eV was found. The explored results suggested that sputtered CdSe thin film deposited at 300 °C has the potential to be used as a window layer in solar cells.

Keywords: cadmium selenide (CdSe); RF magnetron sputtering; window layer; solar cell; deposition temperature



Citation: Rosly, H.N.; Rahman, K.S.; Abdullah, S.F.; Harif, M.N.; Doroody, C.; Chelvanathan, P.; Misran, H.; Sopian, K.; Amin, N. The Role of Deposition Temperature in the Photovoltaic Properties of RF-Sputtered CdSe Thin Films. *Crystals* **2021**, *11*, 73. <https://doi.org/10.3390/cryst11010073>

Received: 17 December 2020

Accepted: 13 January 2021

Published: 17 January 2021

Publisher's Note: MDPI stays neutral with regard to jurisdictional claims in published maps and institutional affiliations.



Copyright: © 2021 by the authors. Licensee MDPI, Basel, Switzerland. This article is an open access article distributed under the terms and conditions of the Creative Commons Attribution (CC BY) license (<https://creativecommons.org/licenses/by/4.0/>).

1. Introduction

Over the past 10 years, there has been a remarkable improvement in the efficiency of CdTe-based solar cells, from 16.7% to 22.1% [1,2]. Despite these improvements, there was no noteworthy efficiency changes in CdS/CdTe-based solar cells from 2016 to 2020 [2–6]. The highest efficiency for CdTe solar cells is still 22.1%, even though many studies have been reported so far. The most dominant window layer for CdTe solar cells is the n-type CdS [7,8]. However, the exploitation of polycrystalline CdS as a window layer has several drawbacks. CdS thin film has a band gap of 2.42 eV, which causes significant optical absorption in the blue region and reduces the current (J_{sc}) by lowering quantum efficiency [9]. Theoretically, it is transparent to wavelengths of light above 510 nm. Therefore, higher-energy photons produce electron hole pairs (EHPs) in the n-CdS layer. As a result of the significant distance between this layer and the depletion region where the EHPs can be collected, this often contributes to the surface recombination current. A CdS film with a thickness of around 100 nm can absorb about 63% of the incident spectrum that has energy greater than its

band gap. Though thinner CdS films are preferable, they are impractical due to excessive pinhole formation and possible electrical shunting across the heterojunction. Below 70 nm, there is a general degradation in cell performance due to a significant decrease in shunt resistance [10]. This is due to excessive pinhole formation across the heterojunction, which has a negative effect on the device fill factor (FF) and open-circuit voltage (Voc) [10]. Based on these limitations, researchers are trying to find a new window layer.

Cadmium selenide (CdSe) is a combination of Cadmium (Cd) from group 2 and Selenium (Se) from group 6. It is an n-type semiconductor. CdSe thin films can be utilized for photovoltaic applications because of a suitable direct band gap of about 1.74 eV for bulk CdSe material, good electrical conductivity, and high absorption [11–13]. Different techniques, such as RF magnetron sputtering, chemical bath deposition (CBD), thermal evaporation, pulsed laser deposition (PLD), electrodeposition, and spray pyrolysis have been applied so far in depositing CdSe thin films [14]. Each technique has its capabilities and advantages in thin-film growth. Of these methods, the RF sputtering technique is seen as a good choice because it allows the depositing of films without ion damage over a large area with uniformity and precision [15].

In recent years, utilization of CdSe thin films as the window layer in CdTe solar cells has been reported. Recent work has stated that the modification of the device structure between the CdS and CdTe layers with an addition of CdSe layers would result in the formation of a $\text{CdTe}_{1-x}\text{Se}_x$ phase with a lower band gap than CdTe [16]. The narrow band gap close to the CdSe/CdTe interface improves device performance. Moreover, it can potentially intensify the carrier lifetime through band gap grading [16]. By incorporating a wider band gap CdSe layer, performance losses are expected to be eliminated, providing the opportunity to investigate variations with different CdSe thicknesses. The efficiency of CdTe solar cells benefits mostly from an improvement in short-circuit current densities (J_{sc}) in the short wavelength regions. Nevertheless, J_{sc} can be enhanced in both short- and long-wavelength regions by incorporating CdSe as a window layer. Comparing to CdS, CdSe has a higher solubility in CdTe, in which a stronger interdiffusion occurs at the CdSe/CdTe interface. Though CdSe has a narrower band gap (~1.7 eV) than CdS (2.4 eV), the development of current collection in the short-wavelength regions can still be attained by optimizing the thickness of the CdSe layer [17]. The standard CdS/CdTe device architecture is incompatible with Se incorporation due to large optical losses. The use of a 1.7 eV band gap CdSe layer seems counterintuitive, as the increased optical absorption in this layer would act to reduce the short-circuit density (J_{sc}) compared to CdS, if the absorption is also parasitic. However, it has been demonstrated that during cell processing, the CdSe diffuses into the CdTe, converting it from a photoinactive CdSe (wurtzite) phase to a photoactive $\text{CdTe}_{1-x}\text{Se}_x$ (zincblende) structure [17]. Larger solubility in CdTe occurs in Se due to a lower size mismatch with tellurium than sulfur. Due to the bowing effect, the energy gap in $\text{CdTe}_{1-x}\text{Se}_x$ is smaller compared to CdTe films. Other than that, photocurrent enhancement in both short- and long-wavelength regions is due to the Se diffusion into the CdTe provided by the CdSe layer [14]. To fabricate solar cells, each layer, from top to bottom, is interconnected. It has taken more than 40 years to optimize CdS as a window layer, but research related to CdS window layers is nearing a saturation level. New materials, such as CdSe, have been introduced as an alternative to be used as the window layer in Cd-based solar-cell applications.

To improve the efficiency of solar cells, each layer needs to be optimized. One of the layers that contributes an increase in efficiency is the window layer. In this paper, the CdSe window layer was studied especially on the aspects of structural, morphological, optical, and electrical properties. Electrical properties for CdSe thin-film window layers are very important in enhancing the efficiency of CdTe solar cells, but very little research has been performed in this area. Most electrical properties are determined for a full-cell device using an I-V measurement. Table 1 shows some groups of researchers who have successfully improved the performance of a device using CdSe. J-V parameters of devices containing CdSe and non-CdSe devices were compared. In general, J_{sc} can be improved

by reducing the band gap or removing the CdS layer. However, one of the causes of Voc losses is reduced band gaps. Interface recombination is also a cause of Voc losses, along with fill-factor losses, but this has not been investigated further. Deposition methods are also listed, as they can affect device performance and material properties. This indicates that, even when using the same CdSe material as the window layer, the results differed depending on the optimization performed during deposition.

Table 1. A comparison of JV parameters of CdSe and non-CdSe devices.

Device Structure	Efficiency [%]	FF [%]	Voc [mV]	Jsc [mA/cm ²]	Source
CdSe (100 nm, RFMS)/ CdTe(CSS)	12.6	60.2	770	27	Poplawsky et al. [16]
CdS (100 nm, RFMS)/ CdTe(CSS)	14.5	75.4	810	23.8	
CdSe (100 nm, RFMS)/ CdTe (CSS)	12.1	64.8	690	26.9	Mia et al. [18]
CdS (140 nm, RFMS)/ CdTe (CSS)	14.6	70	847	24.7	
CdSe (100 nm, RFMS)/ CdTe (CSS)	14.7	69.4	771	27.5	Paudel and Yan [17]
CdS (15 nm, RFMS)/ CdSe (100 nm, RFMS)/ CdTe (CSS)	14.1	64.1	806	27.2	
CdS (130 nm, RFMS)/ CdTe (CSS)	14.8	75.5	811	24.2	
CdS (30 nm, HVE)/ CdSe (60 nm, HVE)/ CdTe (HVE)	12.2	67	710	25.6	Lingg et al. [19]
CdS (120 nm, HVE)/ CdTe (HVE)	10.5	69.4	830	18.5	

Note: RFMS = radio frequency magnetron sputtering; CSS = close-spaced sublimation; HVE = high-vacuum evaporation.

Therefore, when considering the above issues, this paper explores the prospects of CdSe as a window layer instead of the conventional CdS, which will assist in attaining better device performance in the future. The micro-structural and opto-electrical characteristics were analyzed and optimized for CdSe thin films as a possible window layer in solar-cell applications.

2. Experimental Details

2.1. CdSe Thin Film Growth

Borosilicate glass substrates with dimensions of 3 cm × 3 cm and a thickness of 1.1 mm were used in this study. Initially, the substrates were cleaned using acetone, methanol, and deionized water in an ultrasonic bath. CdSe films with a thickness of approximately 100 nm were grown by sputtering at various temperatures. Sputtering deposition of thin films typically involves gases such as argon (Ar) in the chamber and energetic electric cathodes that produce self-sustaining plasma. The CdSe target purity was 99.95% and the target size was 5 cm, as purchased from Matsurf Technologies Inc. (St Paul, MN, USA). The sputtering chamber was evacuated to a base pressure of 1.5×10^{-5} Torr via both mechanical and turbo-molecular pumps. When the deposition process was performed, the deposition pressure reading was taken at an average reading of 2.0×10^{-2} Torr. Figure 1 shows that the error bars overlap at each base pressure, as well as at the deposition pressure. This indicates that most of the base and deposited pressures were almost identical. The substrate was set to the deposition temperature. Ar gas was used as an ambient due to

its low reactivity and high sputter yield. A Kurt J. Lesker 4-gun model radio frequency (RF) magnetron sputtering system equipped with an in-situ substrate holder heated by four quartz halogen lamps from underneath was used for the CdSe deposition. The target-to-substrate distance (sputter down) and RF power were set at approximately 14 cm and 40 watts, respectively. Prior to the deposition, substrates inserted in the chamber were left through a pre-heating process at a set temperature for one hour to prevent non-uniform heating during the deposition process. The deposition temperatures were 25 °C, 100 °C, 200 °C, 300 °C and 400 °C, respectively. Table 2 shows the deposition conditions for the CdSe thin film growth.

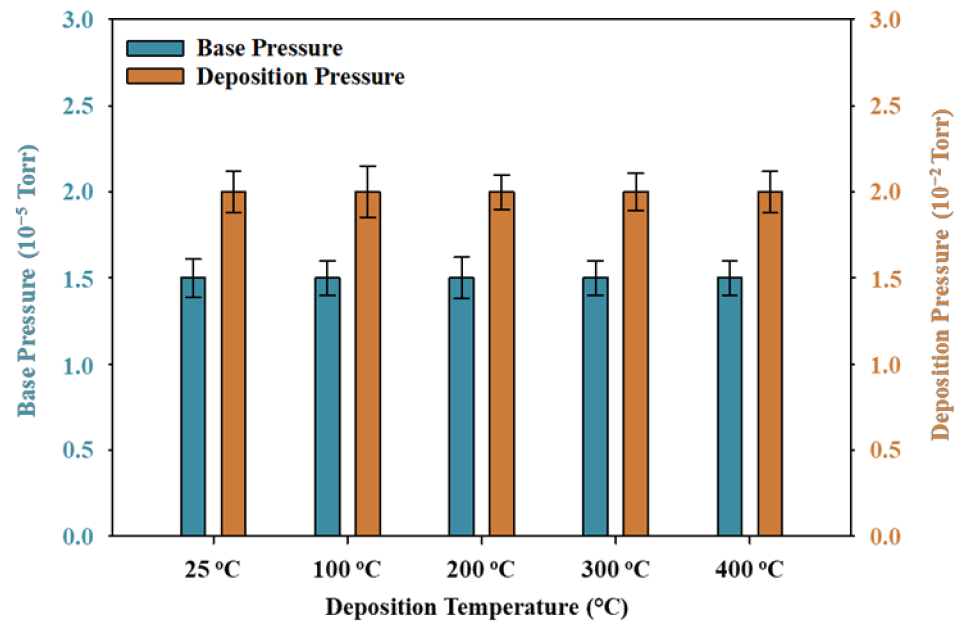


Figure 1. Base and deposition pressures of CdSe thin films at different temperatures.

Table 2. Deposition parameters of the sputtered CdSe thin film.

Parameter	Condition
RF power	40 watts
Ar gas flow	5 SCCM
Deposition time	15 min
Base pressure	1.5×10^{-5} Torr
Deposition pressure	2.0×10^{-2} Torr
Deposition temperature	25 °C, 100 °C, 200 °C, 300 °C, 400 °C

2.2. CdSe Thin Film Characterization

The structural properties and phases were inspected by X-ray diffraction (XRD, Shimadzu, Kyoto, Japan) using a Shimadzu XRD-6000 X-ray diffractometer (employing Cu K α radiation) at room temperature. A surface profiler (Veeco Dektak 150) was used to measure the film thickness. The surface morphology images and grain size were obtained with a Carl Zeiss Merlin field emission scanning electron microscopy (FESEM, Carl Zeiss, Oberkochen, Germany) that was operated at an accelerating voltage of 15 kV. The optical analysis was carried out using a Perkin-Elmer Lambda-35 (UV-Vis, PerkinElmer, Waltham, MA, USA) spectrophotometer. The electrical characteristics were determined by Hall effect measurement using an ECOPIA HMS-3000 system.

3. Result and Discussions

3.1. XRD Analysis

The crystal structure of the CdSe films was investigated using X-ray diffraction patterns. This information was extracted using a Shimadzu XRD-6000 X-ray diffractometer with a Cu-K α monochromator of wavelength $\lambda = 1.54 \text{ \AA}$. The X-ray generator tension was set to 40 kV while the current was adjusted to 40 mA. A range of 2θ from 20° to 80° with a step size of 0.01° pattern was scanned, so that possible diffraction peaks could be detected. An interval of 10 s at each fixed value of 2θ was found sufficient to yield a reasonable number of counts, and therefore an accurate determination of the peak intensities. The purpose of the XRD characterization was to study the effect of different deposition temperatures on the structural and crystallographic properties of the sputtered CdSe film. The XRD patterns of the CdSe films are shown in Figure 2.

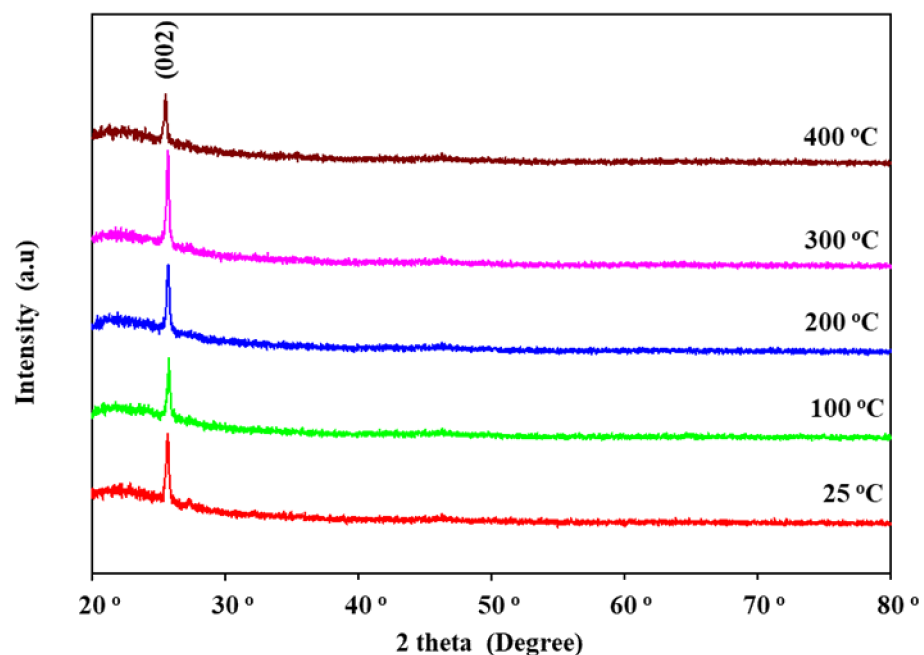


Figure 2. XRD patterns of CdSe thin films.

The CdSe thin film contained polycrystalline features along the (002) plane originated at $2\theta = 24.12^\circ$ for all the temperatures, indicating a hexagonal structure. The structure of CdSe is highly dependent on the sample preparation method, as well as the process or technique used to deposit CdSe. It has been investigated that chemically deposited CdSe films show cubic, hexagonal, or mixed (cubic + hexagonal) crystal structures, depending upon the deposition conditions [20]. CdSe thin films grown by CBD [21] were reported to have a cubic structure, while the electrodeposition method [22] produced a hexagonal structure. In addition, it has been reported that the same deposition method could exhibit different (amorphous/hexagonal) structures [13,23]. After using the sputtering method, an amorphous structure was reported by Chunxiu et al. [14], while a cubic structure has been found in other studies [24]. Although the sputtering method demonstrates different structures, the use of appropriate temperature ensures that CdSe thin films will have a hexagonal structure [14]. In our study, all samples displayed a hexagonal structure, and the peak intensity exhibited an increasing trend as the temperature rose to 300°C . The sample deposited at 300°C showed the strongest preferred (002) orientation. A declining tendency was visible in the peak intensity after 300°C , which could be related to the decrease of surface mobility on glass surfaces and the successive growth of a thin layer of material, as reported by Chander et al. [25]. All of the XRD peaks matched with the JCPDS (card no. 01-075-5680) [26]. Vegard's law [$a_{\text{cubic}} = d_{\text{hkl}} (h^2 + k^2 + l^2)^{1/2}$] and Bragg's formula [$d_{\text{(hkl)}} = (\lambda/2)\text{cosec}\theta$] were used to calculate the lattice constant [27]. Scherrer's formula

$[D_{hkl} = 0.9\lambda/(\beta\cos\theta)]$ and the full width at half maximum (FWHM) of the (002) peak were used to calculate the crystallite size (D) [28]. Crystallinity had a very good correlation with FWHM values. Higher values of FWHM signify a decrease in crystallinity, whereas larger crystal sizes denote an increase in film crystallinity [9]. The microstrain (ϵ) was determined by the equation $[\epsilon = \beta/4\tan\theta]$ [29]. A lower microstrain value signifies monocrystalline property. In contrast, a higher microstrain indicates polycrystalline film. The dislocation density was calculated using Williamson and Smallman's formula $[\delta = n/D^2]$ [30]. Table 3 shows all the computed values for the structural parameters of the CdSe films.

Table 3. Structural parameters of CdSe thin films.

Deposition Temperature	hkl	C (Å)	D_{hkl} (nm)	D (nm)	ϵ [$\times 10^{-3}$]	δ [$\times 10^{11}$] (cm^{-2})
25 °C	(002)	6.947	0.3474	33.964	4.602	0.867
100 °C	(002)	6.922	0.3461	33.970	4.585	0.867
200 °C	(002)	6.941	0.3469	36.391	4.291	0.755
300 °C	(002)	6.939	0.3470	38.818	4.022	0.664
400 °C	(002)	6.988	0.3494	31.831	4.940	0.987

The average crystallite grain sizes ranged between 30–40 nm. A maximum crystallite size of 38.82 nm was obtained for the films deposited at 300 °C. Larger crystallites caused narrowing in FWHM and a strong interface between the film and the substrate. A large grain size indicated good crystallization, which improves the performance of a device, showing that CdSe is a good candidate for the window layer [27]. In the XRD results, there was an increase in intensity from 25 °C to 300 °C, and a decline at 400 °C. The CdSe film grown at 400 °C showed the smallest crystallite size. The discrete crystallite size above 300 °C was the result of changes in the crystal structure of the CdSe film, which specifies a grain rearrangement [14]. Se evaporation could also be detected in many cases during CdSe film growth via sputtering at high temperatures. Se loss could be caused by the decomposition reaction of CdSe, which occurs when the partial pressure of Se is low. The loss of Se might be more evident at 400 °C, and eventually the crystallite sizes decline. Though XRD can provide an approximation of the grain size, its actual assessment could be done via SEM analysis, which determines the grain growth. Figure 3 shows the CdSe thin-film lattice constant deposited at different temperatures, and the error bars overlap at all temperatures. This indicates that the difference was not statistically significant. An average lattice constant of 6.95 Å was attained for the CdSe-diffracted peaks, which agrees with previous works [31,32].

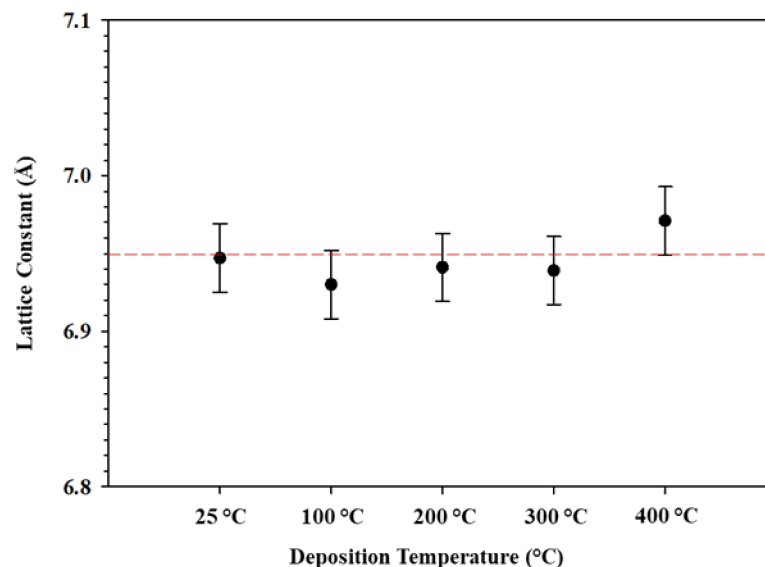


Figure 3. The lattice constants of CdSe thin films grown at different temperatures.

The deposition temperature strongly influenced the dislocation density and microstrain of the CdSe films. Figure 4 shows the changes in the dislocation density and microstrain for various deposition temperatures. The highest dislocation density of $0.99 \times 10^{11} \text{ cm}^{-2}$ was obtained at a 400 °C deposition temperature. The highest value of microstrain of 4.94×10^{-3} was also obtained at the same deposition temperature. At a deposition temperature of 300 °C, the grain size was the highest, while the microstrain and dislocation density were the lowest. This is probably due to lattice disarray and imperfections in the crystal. The imperfection in the crystal, coupled with misregistry of the lattice, could be the causes of the changes in the microstrain and dislocation density.

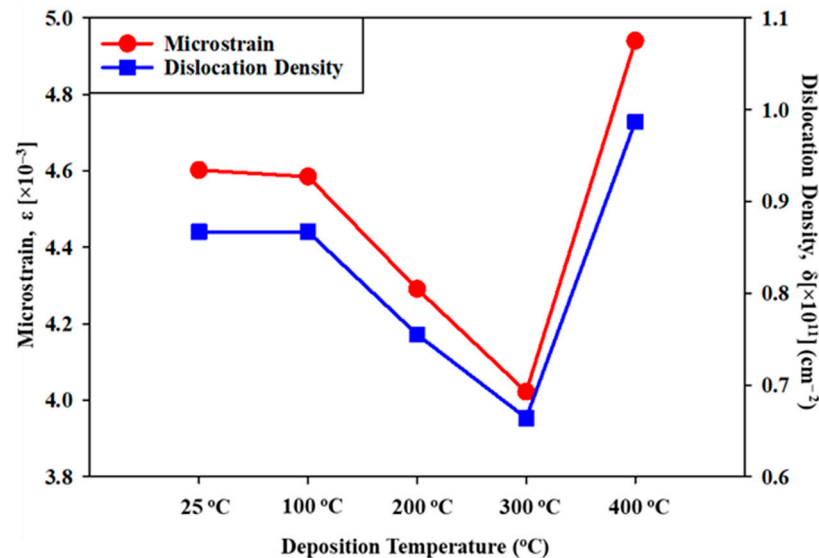


Figure 4. The dislocation density and microstrain variations for the CdSe film.

3.2. FESEM Analysis

FESEM was used to realize the grain growth and surface morphology [31]. Figure 5 displays surface morphology images of the deposited CdSe films. The average grain size and the surface morphology of the films were strongly dependent on the deposition temperature. It was detected in the micrographs that the films had uniform and homogeneous deposition, having identical grains and no cracks or pinholes. The diameter of crystallites was highly dependent on the growth condition. In Figure 6, each rectangle shows the crystallite measurement distribution measured using FESEM, while the horizontal line in the rectangle represents the mean for the crystallite size. There was an increase in grain size at deposition temperatures from 25 °C to 400 °C. However, the error bar at the deposited temperature of 400 °C was long, which indicates that its value was more widespread and less reliable. The grain size was within the range of 26–41 nm, which was comparable with the film thickness, and was well supported by XRD results demonstrated in an earlier study [14]. Smaller grain sizes were observed for films sputtered at lower deposition temperatures, while the maximum grain size was obtained at 400 °C. When the deposition temperature rose from 25 °C to 300 °C, the film remained homogeneous and uniform, but at 400 °C, the particle shape changed from a sphere to an irregular geometric object. As the substrate temperature increased, the particle size also increased. When the substrate temperature was increased to 400 °C, the particles become larger. This is due to grain growth in one direction as the substrate temperature rose, as evidenced by XRD results. The inspected FESEM results matched well with the study presented by Chunxiu et al. [14]. Further optimization is necessary in the CdSe deposition process in order to obtain larger grain sizes. Defects caused by slight changes in thicknesses resulted in variations in the morphology and crystalline structure of the films, due to the rate of element accumulation during film growth [30].

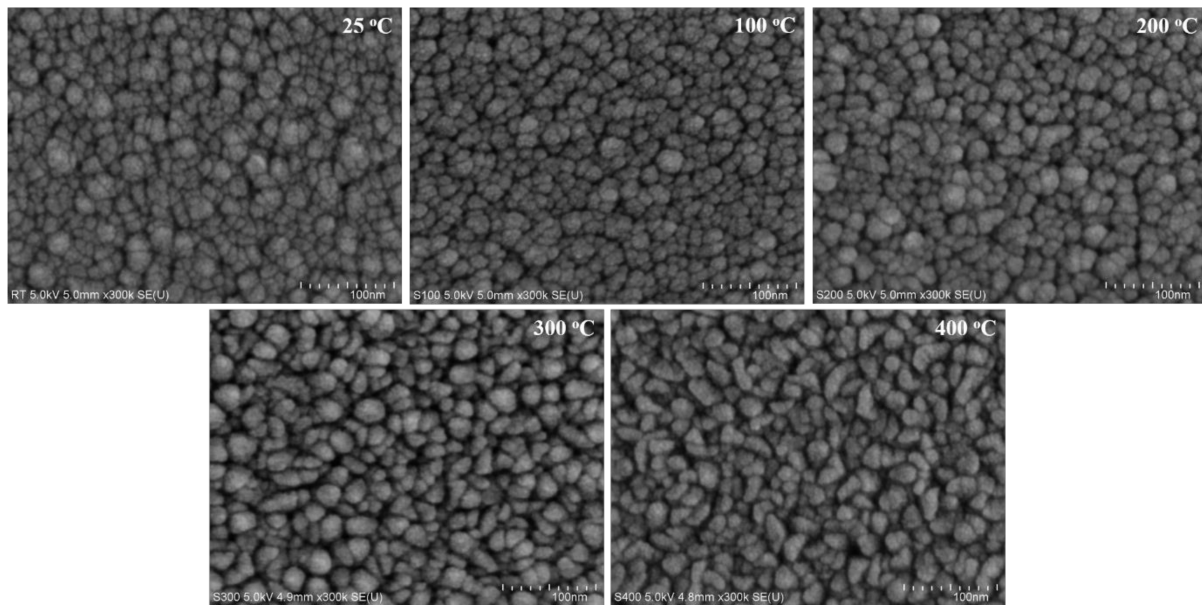


Figure 5. FESEM surface morphology images of the CdSe films.

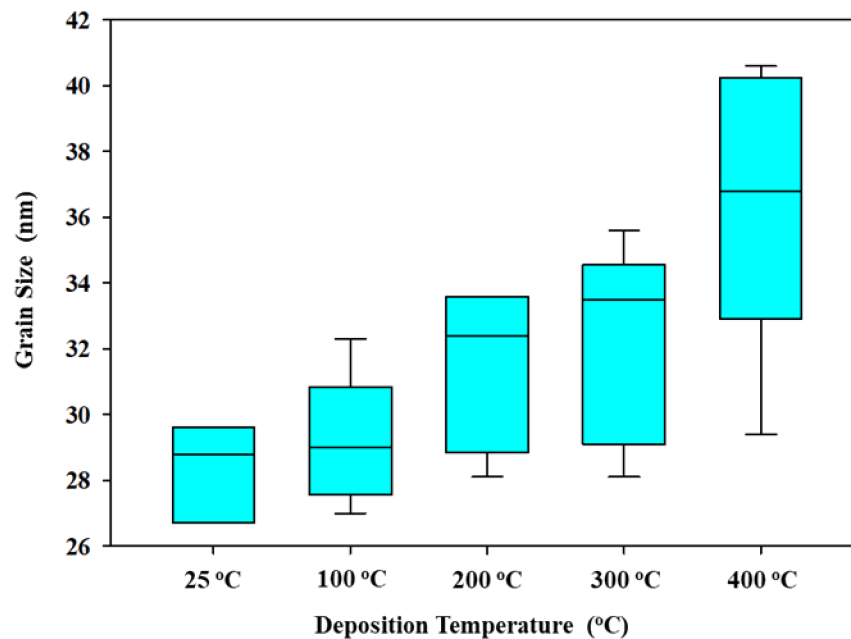


Figure 6. The grain size distribution of the CdSe films at various deposition temperatures.

3.3. Optical Analysis

The optical evaluations were carried out by measuring the optical transmission and band gap of the CdSe films using a UV–Vis spectrometer. Figure 7 shows the transmission spectrum at wavelengths from 325–1000 nm, which revealed that CdSe films can transmit photons at wavelengths at 325 nm and above. Transmission in the wavelength of 300–500 nm was determined to be almost persistent and improved later, with the wavelengths in the higher visible region disclosing the semiconducting property of the films. Within the visible region, the 100 nm CdSe thin film had around 25% higher transmittance than the 300 nm CdSe reported by Chunxiu et al. [14]. This is because at higher thicknesses, the films became dense, which led to decreased transmittance. All the samples were highly transparent in the near-infrared region [24]. Meanwhile, the rise in the transmittance of the films and peak movement of the transmission spectrum to the right with increasing temperature could be attributed to less light scattering due to the better crystal structure

and surface properties, a reduction in voids and lattice imperfections, and an increase in grain size [33].

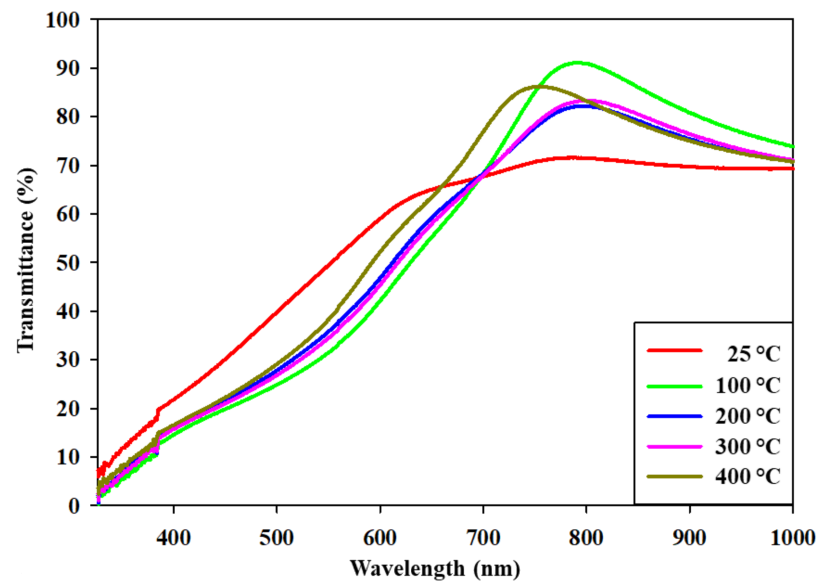


Figure 7. Transmittance spectra of the CdSe thin films grown at different temperatures.

The band gap was extracted using the optical absorbance data by extrapolating the straight line of the graph to the zero absorption coefficient that passed through the energy axis [27]. The band gaps were computed using the formula $[\alpha = A(h\nu - E_g)^{1/2}/h\nu]$ [34,35], where α , $h\nu$, E_g and A denote the absorption coefficient, the photon energy, the band-gap energy, and the constant of proportionality, respectively. A is a constant known as the band-tailing parameter [36]. The plot of $(\alpha h\nu)^2$ vs. $h\nu$ is shown in Figure 8 to find the range of band gaps for the films. The CdSe film was seen to have a direct band gap through the linear nature of the Tauc plot. Optical band gaps were found in the range of 1.65–1.79 eV (Table 4). The results showed that the CdSe films deposited at 100 °C had the lowest E_g of 1.65 eV, while the CdSe film deposited at 25 °C demonstrated the highest E_g of 1.79 eV. All the computed band gaps are well supported by an earlier report [14].

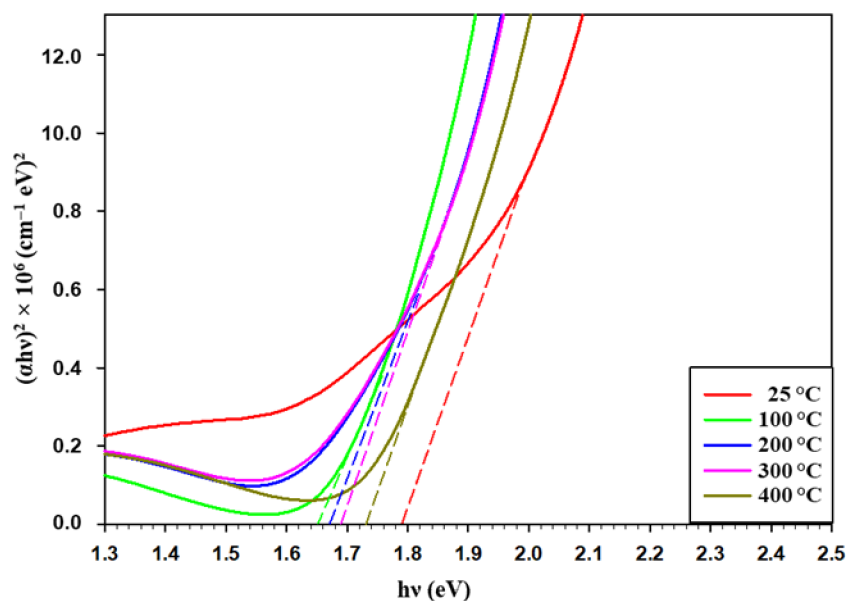


Figure 8. Plot of photon energy ($h\nu$) vs. $(\alpha h\nu)^2$ of the CdSe thin films deposited at different temperatures.

Table 4. CdSe thin-film band gap for various deposition temperatures.

Deposition Temperature	Energy Band Gap (E_g)
25 °C	1.79
100 °C	1.65
200 °C	1.67
300 °C	1.69
400 °C	1.73

3.4. Hall Effect Measurement

A magnetic field of 0.55 T and a probe current of 40 nA were applied to measure the carrier concentration, mobility, and resistivity for the sputtered CdSe films. Table 5 shows the measured electrical values for different deposition temperatures.

Table 5. Electrical parameters of the CdSe thin films.

Deposition Temperature	Carrier Concentration ($/\text{cm}^3$)	Mobility (cm^2/Vs)	Resistivity [$\times 10^3$] ($\Omega \text{ cm}$)	Semiconductor Type
25 °C	3.19×10^{14}	10.13	1.93	n-type
100 °C	4.07×10^{14}	7.32	2.10	n-type
200 °C	5.30×10^{14}	5.66	2.08	n-type
300 °C	9.59×10^{14}	3.21	1.75	n-type
400 °C	2.00×10^{14}	17.38	1.79	n-type

The carrier concentration was obtained in the order of 10^{14} cm^{-3} . Figure 9 shows the significant increase in carrier concentration when the temperature increased from 25 °C to 300 °C during the deposition process. In our study, the deposition of CdSe thin film at a temperature of 300 °C had the highest carrier concentration of $9.59 \times 10^{14} \text{ cm}^{-3}$, which is in line with the results obtained from XRD. This proves that a higher crystallinity caused high carrier concentration. Meanwhile, the carrier concentration increased until 300 °C, and then declined with an increase in the deposition temperature. The films with higher carrier concentration tended to have more carrier-to-carrier scattering due to the augmented chances of carrier impacts, which resulted in lower mobility [37]. The resistivity was found in the order of $10^3 \Omega \text{ cm}$, indicating no significant effect on resistivity by temperature during film growth. Despite that, the lowest resistivity of $1.75 \times 10^3 \Omega \text{ cm}$ was found for the CdSe film deposited at 300 °C. This decrease in resistivity was probably due to the higher carrier concentration resulting from high crystallinity. However, with the increase in the sputtering temperature to 400 °C, and after a highly grown grain structure appeared, the sputtering reaction was transferred from grain growth to a new crystallite-forming reaction within a short time. Under this condition, grain aggregation caused by new crystal nucleus was obvious, as presented by the XRD results. It was determined from the XRD graphs that fast grain nucleation and growth process resulting from a very high sputtering temperature (400 °C in this case) produced small crystallites with misorientations, mismatched lattices, and high strain and stress structures, in agreement with Table 3 and Figure 4. Overall, the mobility was presented to be very high in the CdSe samples grown at 400 °C due to the high grain or particle size shown in the SEM images; nevertheless, the carrier concentration and XRD peak intensity were low due to the lattice mismatch and misoriented crystallinity. Also, high mobility could be due to a decrease in grain boundary-scattering of the charge carriers, which occurs due to an increased particle (grain) size. The results are in line with previous studies [38,39]. Furthermore, numerous methods are available to calculate the diffraction profile, such as the Scherer formula or Williamson-Hall plot [6]. These methods defer in basis, which makes it difficult to compare them directly for a precise grain size estimation [6]. XRD calculates the size of the crystalline domains, while SEM shows physical grains. A single grain can comprise several domains with dissimilar orientations.

Therefore, the grain size measured by SEM will be always larger or, in case of the perfect grains, equal to that calculated by XRD [6]. Consequently, a grain size measured using SEM is an average value, whereas the Scherrer formula calculates the crystallite size using the diffraction information from a single plane at a particular 2θ and FWHM value. Overall, the XRD technique provides the crystallite size present in the grains, while the microscopic study via SEM delivers the average grain size of the material. Since grains encompass many crystallites, the crystallite size and grain size are not same [6]. It is quite challenging to understand and control the carrier concentration, resistivity, and mobility in polycrystalline CdSe films. Intrinsic defects and strong self-compensation are often caused by the ionic bonds between constituent atoms [6]. Therefore, obtaining a low carrier concentration of CdSe is a major challenge to improving thin-film solar cell performance. Electrical properties suggested that the changes in the sputtering temperature had a significant impact on the deposited film properties. An intensification of the deposition temperature improved crystallinity, as seen in the XRD and FESEM results. The results showed that good crystallinity results in lower electrical resistivity. This is probably due to the lower carrier recombination in the grain boundaries.

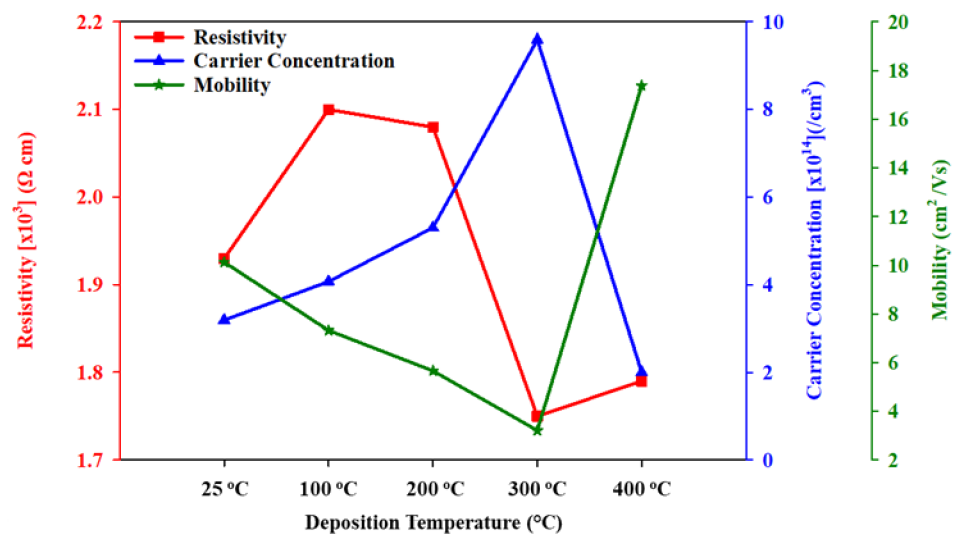


Figure 9. Variations in carrier concentration, mobility, and resistivity in the CdSe thin films.

4. Conclusions

The influence of deposition temperature on the structural and opto-electrical properties of CdSe films was investigated thoroughly to optimize solar-cell applications. The XRD investigation showed that all of the sputtered films demonstrated a polycrystalline nature along the (002) hexagonal plane as their preferential orientation. The CdSe film deposited at 300 °C showed the highest intensity, with its grain size among the largest, ensuring better crystallinity than the other films. The grain size was found in the range of 26–41 nm, which matched well with published literature. All of the samples were highly transparent in the near-infrared region, and the energy band gap attained in our study was within the range of 1.65–1.79 eV. Although the CdSe thin film grown at 400 °C exhibited the highest mobility, the particles changed from spheres to irregular geometric objects, which caused the film to become non-uniform. The highest carrier concentration of $9.59 \times 10^{14} \text{ cm}^{-3}$ was obtained at 300 °C, which coordinated well with the XRD results. The lowest electrical resistivity also was found at a deposited temperature of 300 °C due to the higher crystallinity. All of the properties fit well with the standard reported values. The CdSe film deposited at 300 °C showed the optimum value as a potential window layer in solar-cell applications due to its structure, grain growth, high optical transmission, and apposite electrical properties. Overall, this study scrutinized the viability of CdSe as a window layer, but rigorous investigation and further optimization are needed to incorporate it in CdTe solar-cell devices and improve their efficiency.

Author Contributions: Conceptualization, H.N.R. and K.S.R.; data curation, H.N.R.; formal Analysis, H.N.R. and K.S.R.; funding acquisition, N.A., S.F.A. and K.S.; methodology, H.N.R., K.S.R., M.N.H., C.D. and P.C.; investigation, H.N.R. and K.S.R., M.N.H., P.C. and C.D.; project administration, K.S.R. and N.A.; writing—original draft preparation, H.N.R.; writing—review and editing, K.S.R.; visualization, H.N.R.; validation, K.S.R. and N.A.; supervision, K.S.R., H.M. and N.A. All authors have read and agreed to the published version of the manuscript.

Funding: This work is supported by the Ministry of Higher Education (MOHE), Malaysia through FRGS Grant No. FRGS/1/2018/TK05/UNITEN/02/1.

Institutional Review Board Statement: Not applicable.

Informed Consent Statement: Not applicable.

Data Availability Statement: Not applicable.

Acknowledgments: Authors are indebted to the Institute of Sustainable Energy (ISE) of the Universiti Tenaga Nasional (@The Energy University) and Universiti Kebangsaan Malaysia (@The National University of Malaysia) for laboratory support.

Conflicts of Interest: The authors declare no conflict of interest.

References

- Gloeckler, M.; Sankin, I.; Zhao, Z. CdTe Solar Cells at the Threshold to 20% Efficiency. *IEEE J. Photovolt.* **2013**, *3*, 1389–1393. [[CrossRef](#)]
- Lai, H.; Ren, A.; Wu, L.; Hao, X.; Zhang, J.; Wang, W.; Wei, Q.; Ni, Z.; Feng, L. Laser scribing of Cd₂SnO₄-based CdTe polycrystalline solar cells. *Renew. Energy* **2020**, *145*, 133–140. [[CrossRef](#)]
- Salavei, A.; Menossi, D.; Piccinelli, F.; Kumar, A.; Mariotto, G.; Barbato, M.; Meneghini, M.; Meneghesso, G.; Di Mare, S.; Mariotto, G.; et al. Comparison of high efficiency flexible CdTe solar cells on different substrates at low temperature deposition. *Sol. Energy* **2016**, *139*, 13–18. [[CrossRef](#)]
- García-Alvarado, G.; De Moure-Flores, F.; Mayén-Hernández, S.; Santos-Cruz, D.; Rivera-Muñoz, E.; Contreras-Puente, G.; Pal, M.; Santos-Cruz, J. CdTe/CdS solar cells with CdTe grown at low vacuum. *Vacuum* **2017**, *142*, 175–180. [[CrossRef](#)]
- Bosio, A.; Rosa, G.; Romeo, N. Past, present and future of the thin film CdTe/CdS solar cells. *Sol. Energy* **2018**, *175*, 31–43. [[CrossRef](#)]
- Rahman, K.S.; Harif, M.N.; Rosly, H.N.; Bin Kamaruzzaman, M.I.; Akhtaruzzaman, M.; Alghoul, M.; Misran, H.; Amin, N. Influence of deposition time in CdTe thin film properties grown by Close-Spaced Sublimation (CSS) for photovoltaic application. *Results Phys.* **2019**, *14*, 102371. [[CrossRef](#)]
- Ferekides, C.; Balasubramanian, U.; Mamazza, R.; Viswanathan, V.; Zhao, H.; Morel, D. CdTe thin film solar cells: Device and technology issues. *Sol. Energy* **2004**, *77*, 823–830. [[CrossRef](#)]
- McCandless, B.E.; Dobson, K.D. Processing options for CdTe thin film solar cells. *Sol. Energy* **2004**, *77*, 839–856. [[CrossRef](#)]
- Islam, M.A.; Rahman, K.S.; Sobayel, K.; Enam, T.; Ali, A.M.; Zaman, M.; Akhtaruzzaman, M.D.; Amin, N. Fabrication of high efficiency sputtered CdS: O/CdTe thin film solar cells from window/absorber layer growth optimization in magnetron sputtering. *Sol. Energy Mater. Sol. Cells* **2017**, *172*, 384–393. [[CrossRef](#)]
- Kephart, J.; McCamy, J.; Ma, Z.; Ganjoo, A.; Alamgir, F.; Sampath, W. Band alignment of front contact layers for high-efficiency CdTe solar cells. *Sol. Energy Mater. Sol. Cells* **2016**, *157*, 266–275. [[CrossRef](#)]
- El-Menyawy, E.; Azab, A.A. Optical, electrical and photoelectrical properties of nanocrystalline cadmium selenide films for photosensor applications. *Optik* **2018**, *168*, 217–227. [[CrossRef](#)]
- Mathuri, S.; Ramamurthi, K.; Babu, R.R. Influence of deposition distance and substrate temperature on the CdSe thin films deposited by electron beam evaporation technique. *Thin Solid Film.* **2017**, *625*, 138–147. [[CrossRef](#)]
- Sahebi, R.; Roknabadi, M.R.; Behdani, M. Semi-transparent Schottky junction solar cell based on evaporated CdSe thin films: Influence of post-deposition air-annealing. *Optik* **2020**, *204*, 164204. [[CrossRef](#)]
- Li, C.; Wang, F.; Chen, Y.; Wu, L.; Zhang, J.; Li, W.; He, X.; Li, B.; Feng, L. Characterization of sputtered CdSe thin films as the window layer for CdTe solar cells. *Mater. Sci. Semicond. Process.* **2018**, *83*, 89–95. [[CrossRef](#)]
- Islam, M.A.; Rahman, K.S.; Haque, F.; Khan, N.A.; Akhtaruzzaman, M.; Alam, M.M.; Ruslan, H.; Sopian, K.; Amin, N. Effect of Sn Doping on the Properties of Nano-Structured ZnO Thin Films Deposited by Co-Sputtering Technique. *J. Nanosci. Nanotechnol.* **2015**, *15*, 9184–9191. [[CrossRef](#)]
- Poplawsky, J.D.; Guo, W.; Paudel, N.; Ng, A.; More, K.; Leonard, D.; Yan, Y. Structural and compositional dependence of the CdTe_xSe_{1-x} alloy layer photoactivity in CdTe-based solar cells. *Nat. Commun.* **2016**, *7*, 12537.
- Paudel, N.R.; Yan, Y. Enhancing the photo-currents of CdTe thin-film solar cells in both short and long wavelength regions. *Appl. Phys. Lett.* **2014**, *105*, 183510. [[CrossRef](#)]
- Mia, D.; Swartz, C.H.; Paul, S.; Sohal, S.; Grice, C.R.; Yan, Y.; Holtz, M.; Li, J.V. Electrical and optical characterization of CdTe solar cells with CdS and CdSe buffers—A comparative study. *J. Vac. Sci. Technol. B* **2018**, *36*, 052904. [[CrossRef](#)]

19. Lingg, M.; Spescha, A.; Haass, S.G.; Carron, R.; Buecheler, S.; Tiwari, A.N. Structural and electronic properties of CdTe_{1-x}Se_x films and their application in solar cells. *Sci. Technol. Adv. Mater.* **2018**, *19*, 683–692. [[CrossRef](#)]
20. Yadav, A.; Barote, M.; Masumdar, E. Studies on cadmium selenide (CdSe) thin films deposited by spray pyrolysis. *Mater. Chem. Phys.* **2010**, *121*, 53–57. [[CrossRef](#)]
21. Elahi, M.; Ghobadi, N. Structural, Optical and Electrical Properties of CdSe Nanocrystalline Films. *Iranian Phys. J.* **2008**, *2*, 27–31.
22. Mahato, S.; Shakti, N.; Kar, A. Annealing temperature dependent structural and optical properties of electrodeposited CdSe thin films. *Mater. Sci. Semicond. Process.* **2015**, *39*, 742–747. [[CrossRef](#)]
23. Sarmah, K.; Sarma, R.; Das, H.L. Structural characterization of thermally evaporated CdSe thin films. *Chalcogenide Lett.* **2008**, *5*, 153–163.
24. Wang, A.; Li, C.; Zhang, J.; Wu, L.; Wang, W.; Feng, L. Annealing temperature dependence of properties of CdSe thin films by RF-sputtering. In *IOP Conference Series: Materials Science and Engineering*; IOP Publishing: Bristol, UK, 2019; Volume 556, p. 012006.
25. Chander, S.; Dhaka, M. Enhancement in microstructural and optoelectrical properties of thermally evaporated CdTe films for solar cells. *Results Phys.* **2018**, *8*, 1131–1135. [[CrossRef](#)]
26. Kitazono, K.; Akashi, R.; Fujiwara, K.; Akita, A.; Naya, S.I.; Fujishima, M.; Tada, H. Photocatalytic Synthesis of CdS (core)–CdSe (shell) Quantum Dots with a Heteroepitaxial Junction on TiO₂: Photoelectrochemical Hydrogen Generation from Water. *ChemPhysChem* **2017**, *18*, 2840–2845. [[CrossRef](#)]
27. Haque, F.; Rahman, K.S.; Akhtaruzzaman; Abdullah, H.; Kiong, T.S.; Amin, N.; Tiong, S.K. Properties of sputtered ZnS thin films for photovoltaic application. *Mater. Res. Express* **2018**, *5*, 096409. [[CrossRef](#)]
28. Khan, N.; Rahman, K.; Aris, K.; Ali, A.; Misran, H.; Akhtaruzzaman, M.; Tiong, S.; Amin, N. Effect of laser annealing on thermally evaporated CdTe thin films for photovoltaic absorber application. *Sol. Energy* **2018**, *173*, 1051–1057. [[CrossRef](#)]
29. Harif, M.N.; Rahman, K.S.; Rosly, H.N.; Chelvanathan, P.; Doroody, C.; Misran, H.; Amin, N. An approach to alternative post-deposition treatment in CdTe thin films for solar cell application. *Superlattices Microstruct.* **2020**, *147*, 106687. [[CrossRef](#)]
30. Rosly, H.N.; Rahman, K.S.; Harif, M.N.; Doroody, C.; Isah, M.; Misran, H.; Amin, N. Annealing temperature assisted microstructural and optoelectrical properties of CdSe thin film grown by RF magnetron sputtering. *Superlattices Microstruct.* **2020**, *148*, 106716. [[CrossRef](#)]
31. Murali, K.; Sivaramamoorthy, K.; Kottaisamy, M.; Bahadur, S.A. Photoconductive studies on electron beam evaporated CdSe films. *Phys. B Condens. Matter* **2009**, *404*, 2449–2454. [[CrossRef](#)]
32. Patel, S.; Purohit, A.; Chander, S.; Kannan, M.; Dhaka, M. An approach to MgCl₂ activation on CdSe thin films for solar cells. *Curr. Appl. Phys.* **2018**, *18*, 803–809. [[CrossRef](#)]
33. Göde, F.; Ünlü, S. Synthesis and characterization of CdS window layers for PbS thin film solar cells. *Mater. Sci. Semicond. Process.* **2019**, *90*, 92–100. [[CrossRef](#)]
34. Islam, M.A.; Rahman, K.S.; Haque, F.; Dhar, N.; Salim, M.; Akhtaruzzaman, M.; Sopian, K.; Amin, N. Opto-electrical properties of in doped CdS thin films by co-sputtering technique. *J. Ovonic Res.* **2014**, *10*, 185–190.
35. Gorji, N.E. Oxygen incorporation into CdS/CdTe thin film solar cells. *Opt. Quantum Electron.* **2015**, *47*, 2445–2453. [[CrossRef](#)]
36. Khomchenko, A.V.E. *Waveguide Spectroscopy of Thin Films*; Elsevier: Amsterdam, The Netherlands, 2005.
37. Mendoza, M.F.; Pérez, R.C.; Torres-Delgado, G.; Marín, J.M.; Orea, A.C.; Zelaya-Angel, O. Structural, morphological, optical and electrical properties of CdTe films deposited by CSS under an argon–oxygen mixture and vacuum. *Sol. Energy Mater. Sol. Cells* **2011**, *95*, 2023–2027. [[CrossRef](#)]
38. Akbarnejad, E.; Ghorannevis, Z.; Abbasi, F.; Ghorannevis, M. Investigation of annealing temperature effect on magnetron sputtered cadmium sulfide thin film properties. *J. Appl. Phys.* **2016**, *11*, 45–49. [[CrossRef](#)]
39. Das, N.; Chakrabartty, J.; Farhad, S.; Gupta, A.S.; Ahamed, E.I.; Rahman, K.; Wafi, A.; Alkahtani, A.; Matin, M.; Amin, N. Effect of substrate temperature on the properties of RF sputtered CdS thin films for solar cell applications. *Results Phys.* **2020**, *17*, 103132. [[CrossRef](#)]